

Dynamics of vortex lines in the three-dimensional complex Ginzburg-Landau equation: Instability, stretching, entanglement, and helices

I. S. Aranson,^{1,2} A. R. Bishop,³ and L. Kramer⁴

¹Argonne National Laboratory, 9700 South Cass Avenue, Argonne, Illinois 60439

²Department of Physics, Bar Ilan University, Ramat Gan 52900, Israel

³Theoretical Division and Center for Nonlinear Studies, Los Alamos National Laboratory, Los Alamos, New Mexico 87545

⁴Department of Physics, University of Bayreuth, Bayreuth 95440, Germany

(Received 8 December 1997)

The dynamics of curved vortex filaments is studied analytically and numerically in the framework of a three-dimensional complex Ginzburg-Landau equation (CGLE). It is shown that a straight vortex line is unstable with respect to spontaneous stretching and bending in a substantial range of parameters of the CGLE, resulting in formation of persistent entangled vortex configurations. The boundary of the three-dimensional instability in parameter space is determined. Near the stability boundary, the supercritical saturation of the instability is found, resulting in the formation of stable helicoidal vortices. [S1063-651X(98)01805-4]

PACS number(s): 05.45.+b, 47.20.Ky, 47.27.Eq

I. INTRODUCTION

Analysis of “universal” models plays a central role in contemporary nonlinear dynamics. Such models, as with Ginzburg-Landau and Swift-Hohenberg equations, allow for a quantitative description of arbitrary nonlinear system at the threshold of specific instabilities. The complex Ginzburg-Landau equation (CGLE), derived some 20 years ago by Newell [1] and Kuramoto [2], has become a paradigm model for a qualitative description of weakly nonlinear oscillatory media (for a review, see Ref. [3]). Under appropriate scaling of the physical variables, the equation assumes the universal form

$$\partial_t A = A - (1 + ic)|A|^2 A + (1 + ib)\Delta A, \quad (1)$$

where A is the complex amplitude, b and c are real parameters, and $\Delta = \partial_x^2 + \partial_y^2 + \partial_z^2$ is a three-dimensional Laplace operator. The parameter b is the ratio of dispersion to diffusion, and c is the ratio of conservative to dissipative nonlinearity. Although the equation is formally valid only at the threshold of a supercritical Hopf bifurcation, it has been found that the CGLE often reproduces qualitatively correct phenomenology over a much wider range of the parameters. As a result, the predictions drawn from the analysis of the CGLE (mostly in one and two spatial dimensions; see, e.g., Refs. [4–7]) were recently successfully confirmed by experiments in optical and chemical systems [8,9]. Moreover, some results obtained from the CGLE (for example, symmetry breaking of spiral pairs) was instructive for an interpretation of experiments in far more complicated systems of chemical waves [10] and colonies of amoebae [11,12].

In three dimensions the point singularity at the center of the spiral becomes a line singularity, known as a scroll, or vortex filament. The filaments can be open (scrolls), closed (vortex loops and rings), knotted, or even interlinked or entangled. Scroll vortices had been observed in slime mold [13], heart tissues [14], and a gel-immobilized Belousov-Zhabotinskii (BZ) reaction [15]. Long-lived entangled vortex patterns in three-dimensional BZ reactions were observed re-

cently by the group of Winfree using the advanced optical tomography technique [16]. Complicated vortex configurations have also been observed in numerical simulations of reaction-diffusion equations [17–19].

Theoretical investigation of scroll vortices in reaction-diffusion systems was initiated by Keener [20], who derived the equation of motion for the filament axis. In particular, he obtained that the collapse rate is proportional to the local curvature of the filament, leading to a collapse of a vortex ring in a finite time. The existence of nonvanishing vortex configurations and an expansion of vortex loops, also observed in numerical simulations of reaction-diffusion equations, was associated with “negative line tension” of the vortex filament [18].

Recently, the dynamics of *three-dimensional* (3D) vortex lines in the CGLE has attracted substantial attention [21–23]. As a definition of a vortex line, we accept a line singularity of the phase of a complex function A . Gabbay Ott and Guzdar [22] applied a generalization of Keener’s method for a scroll vortex in reaction-diffusion systems [20]. They derived that the ring of a radius R collapses in finite time according to the following evolution law

$$\frac{dR}{dt} = -\frac{1+b^2}{R}. \quad (2)$$

In addition, there is no (at least, in the first order in $1/R$) overall drift of the vortex ring in the direction perpendicular to the collapse motion. The collapse rate (often called “line tension”) $\nu = 1 + b^2$ appears to be in a reasonable agreement with the simulations [22]. This result generalizes Keener’s ansatz by including the curvature-induced shift of the filament’s wave number. Thereby, as follows from Eq. (2), vortex loops initially existing in the system will always shrink (if, of course, there is no bulk instability of the waves emitted by the vortex filament), and under no condition can the vortex loop expand.

In this paper we show that under very general conditions, and in an extensive part of the parameter space, vortex filaments *expand and bend* spontaneously and result in persis-

tent vortex configurations even if there is no bulk instability of the emitted waves, and the spiral wave is stable in a two-dimensional system. A preliminary account of this work was published in Ref. [23]. We have shown that vortex loops may expand for any value of b above some critical value $b_c(c)$. The critical value $b_c(c)$ can be relatively small for not too large c . For example, our analysis predicts that $b_c \approx 2$ for $c=0$. We prove that, for $b > b_c$ Eq. (2) is not valid, because formally higher-order, but in fact singular, corrections, omitted in Eq. (2), cause severe instability of the filament and persistent stretching. This instability is a three-dimensional manifestation of the two-dimensional core instability of spiral waves (called *acceleration instability* in Ref. [6]). Its origin can be traced back to the breakdown of the Galilean invariance of the CGLE for any $\epsilon = 1/b \neq 0$, causing spontaneous acceleration of the spiral waves [6]. Whereas in two dimensions the instability is relatively weak, the situation is different in three dimensions. Using combined analytical and numerical methods, we have proven that the three-dimensional instability of the vortex filaments persists far beyond the core instability limit of a two-dimensional spiral wave, and typically has a much higher growth rate. It ceases to exist only when the core modes becomes strongly damped. This instability is not driven by “negative line tension.” It develops from a nontrivial response of the filament core to bending, which results in additional “acceleration” terms in the equation of filament motion. As we will show, the bending of the filament greatly enhances the instability, and may result in the formation, after some transient, of a highly entangled and dense vortex configuration. The “high dispersion limit” $b \gg 1$ is readily fulfilled for many physical and chemical systems (actually b larger than about 2 is enough to have the effect). For example, in the context of nonlinear optics, where the CGLE can be derived from the Maxwell-Bloch equation in the good cavity limit [24], this parameter is very small: $\epsilon = 1/b \sim 10^{-4} - 10^{-3}$. For an oscillating chemical reaction the diffusion rates of various reacting components can be varied over a wide range by adding extra chemicals.

The structure of this paper is the following. In Sec. II we present an analysis of the filament motion in the “high dispersion” limit $\epsilon = 1/b \ll 1$. This allows us to prove the instability of a straight vortex filament with respect to bending and stretching on the basis of a computer-assisted analytical procedure. In Sec. III, we present the results of numerical simulations of the three-dimensional CGLE. We discuss the properties of a spatiotemporal intermittency which we have found in our simulations. In Sec. IV, we consider the formal stability analysis of a straight vortex filament with respect to periodic perturbations along the filament axes. Using a numerical matching-shooting algorithm, we have calculated the spectrum of eigenvalues, and determined the stability limit of a three-dimensional vortex line in the b, c plane. In Sec. V, we present a weakly nonlinear analysis for the vortex filament near the three-dimensional stability limit showing the existence of traveling helix solutions. After some concluding remarks in Sec. VI we present in the Appendix an analytical derivation of the equation of motion of the vortex line and the stability boundary in the limit of the perturbed nonlinear Schrödinger equation (NSE).

II. INSTABILITY OF WEAKLY CURVED FILAMENTS IN A HIGH DISPERSION LIMIT

A. Derivation of the equation of motion

As a test for instability, we consider the dynamics of a weakly curved vortex filament in the high-dispersion limit $b \gg 1$. We apply the generalization of the method of Ref. [6] for the case of 3D vortices, and make perturbations near the 2D spiral wave solution to the CGLE. For convenience, we redefine $\mathbf{r} \rightarrow \mathbf{r}/\sqrt{b}$. Then Eq. (1) assumes the form

$$\partial_t A = A - (1 + ic)|A|^2 A + (\epsilon + i)\Delta A. \quad (3)$$

In the following discussion in this section, we assume $0 < \epsilon \ll 1$ to be a small parameter. Our objective is to relate the acceleration of the vortex filament $\partial_t \mathbf{v}$ with the velocity \mathbf{v} and local curvature κ of the filament.

In order to develop the perturbation theory for a weakly curved vortex filament in three dimensions, we begin with the stationary one-armed isolated spiral solution to Eqs. (1) and (3), which is of the form

$$A_0(r, \theta) = F(r) \exp\{i[\omega t \pm \theta + \psi(r)]\}, \quad (4)$$

where (r, θ) are polar coordinates, $\omega = -c - k_0^2(1 - \epsilon c)$ is the rotation frequency, and k_0 is an asymptotic wave number. The real functions F and ψ have the asymptotic behaviors $F(r) \rightarrow \sqrt{1 - \epsilon k_0^2}$, $\psi'(r) \rightarrow k_0$ for $r \rightarrow \infty$ and $F(r) \sim r$, $\psi'(r) \sim r$ for $r \rightarrow 0$. The wave number k_0 of the waves emitted by the spiral is determined uniquely for given ϵ, c [25]. For $\epsilon = 0$ one has a type of Galilean invariance and, then, in addition to the stationary spiral, there exists a family of spirals moving with arbitrary constant velocity $\mathbf{v} = (v_x, v_y)$ [6],

$$A(r, t) = F(r') \exp\left[i\omega' t + \theta + \psi(r') + \frac{\mathbf{r}' \cdot \mathbf{v}}{2}\right], \quad (5)$$

where $\mathbf{r}' = \mathbf{r} - \mathbf{v}t$, $\omega' = \omega - \mathbf{v}^2/4$, and the functions F and ψ are those of Eq. (4). (This invariance holds for any stationary solution.) For $\epsilon \neq 0$ the diffusion term $\sim \epsilon \Delta A$ destroys the family, and leads to slow acceleration or deceleration of the spiral proportional to ϵv , depending on the value of ϵ . As found in Ref. [6], the equations of motion of the spiral core for $\epsilon \ll 1$ assume the form

$$\partial_t \mathbf{v} + \epsilon \hat{K} \mathbf{v} = \mathbf{0}, \quad (6)$$

with the “friction” tensor

$$\hat{K} = \begin{pmatrix} K_{xx} & K_{xy} \\ K_{yx} & K_{yy} \end{pmatrix}. \quad (7)$$

Because of isotropy the elements of the tensor satisfy the condition $K_{xx} = K_{yy}$, $K_{xy} = -K_{yx}$. Equation (6) can be written in a more compact form:

$$\partial_t \hat{v} + \epsilon \chi \hat{v} = 0, \quad (8)$$

where $\hat{v} = v_y + i v_x$ is a “complex” velocity and $\chi = K_{xx} + i K_{xy}$ is a “complex” friction coefficient. It was shown in the Ref. [6] that the coefficient $K_{xx} < 0$ for $\epsilon \ll 1$, which implies instability of the spiral core (see Fig. 1). In the limit of

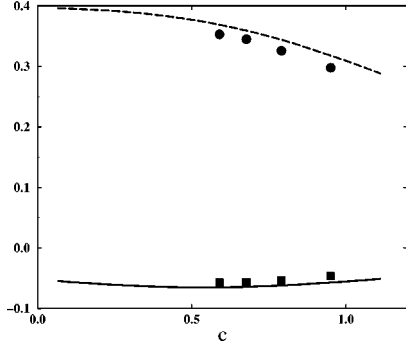


FIG. 1. K_{xx} (solid line) and K_{xy} (dashed line) as functions of c . Lines are theoretical results, and symbols are the results of two-dimensional simulations from Ref. [6] for $\epsilon=0.025$.

the weakly perturbed NSE ($c \rightarrow \infty$), the friction χ is of the form (see Appendix A): $\chi \approx -3.45c^3 \exp[-c\pi](1 \pm i3.92)$. Since in general $K_{xy} \neq 0$, the spiral core moves on a logarithmic spiral trajectory.

Let us now consider the dynamics of an almost straight vortex line. The analysis is conveniently performed in a filament-based coordinate system (for details, see Ref. [22]). The position in space X is represented by local coordinates s , \tilde{x} , and \tilde{y} , where s is the arclength along the filament, and $\mathbf{X} = \mathbf{R}(s) + \tilde{x}\mathbf{N}(s) + \tilde{y}\mathbf{B}(s)$, where \mathbf{R} is the coordinate of the filament, $\mathbf{N}(s)$ the normal, and $\mathbf{B}(s)$ the binormal vector (see also Fig. 1 in Ref. [22]). On this basis the weakly curved filament moving with velocity \mathbf{v} can be written in the form

$$A(r, t) = [F(r') + W(r', \theta, s)] \exp \left[i \left(\omega' t + \theta + \phi_0 + \psi(r') + \frac{\mathbf{r}' \cdot \mathbf{v}}{2} \right) \right]. \quad (9)$$

Here $\mathbf{r}' = \mathbf{r} - \mathbf{v}t$, ϕ_0 is a phase, and W is the perturbation to the spiral solution which we require to be small. We assume that the velocity vector \mathbf{v} lies in the plane perpendicular to the vector tangential to the vortex line, and may in general depend (slowly) on the arclength s . Substituting W into Eq. (3), we obtain at first order in ϵ the linear inhomogeneous (assuming $\partial_t v, v, \kappa \ll 1$ and neglecting higher-order corrections $\partial_s v, \partial_s^2 v$, etc.) equation

$$\hat{L}(W, W^*) = H, \quad (10)$$

where

$$\hat{L}(W, W^*) = i\tilde{\Delta}W + \frac{2i}{r^2} \partial_\theta W + 2iF \frac{\partial W}{\partial r} \frac{1}{F} - (1 + ic)F^2(W + W^*), \quad (11)$$

and $\tilde{\Delta} = \partial_r^2 + (1/r)\partial_r + (1/r^2)\partial_\theta^2 - (1/rF)\partial_r(r\partial_r F)$. The inhomogeneity H is of the form

$$H = \frac{i}{2} \partial_t \mathbf{r} F - i \partial_t \phi_0 F - \epsilon \mathbf{v} [\nabla F + iF \nabla(\theta + \psi)] + \kappa(\epsilon + i) \times [\partial_{\tilde{x}} F + iF \partial_{\tilde{x}}(\theta + \psi)], \quad (12)$$

where (r, θ) are polar coordinates in a local plane spanned on the vectors of normal and binormal, and we used the expansion for the Laplace operator in the local basis in the limit of small curvature κ and torsion τ : $\Delta = -\kappa \partial_{\tilde{x}} + \partial_{\tilde{x}}^2 + \partial_{\tilde{y}}^2 + \partial_s^2 + \dots$. We use the notation $\hat{v} = v_B + iv_N$, where v_B and v_N are the binormal and normal components of the velocity, respectively (note that the coordinate \tilde{x} is directed along the vector of normal).

Separating real and imaginary part of W , and representing it in the form of a Fourier series

$$\begin{pmatrix} \text{Re}W \\ \text{Im}W \end{pmatrix} = \sum_{n=-\infty}^{\infty} \begin{pmatrix} A_n(r) \\ B_n(r) \end{pmatrix} \exp(in\theta), \quad (13)$$

we arrive at the set of ordinary differential equations for each azimuthal modes A_n and B_n . Since instability occurs only for the first azimuthal mode, we consider the equation only for $n=1$ (the equation for $n=-1$ is obtained by complex conjugation). At first order in ϵ the inhomogeneous linear equation for the corrections A_1, B_1 is of the form

$$\begin{aligned} \hat{\Delta}A_1 - 2 \left(cF^2A_1 + \psi'F \frac{\partial B_1}{\partial r} \frac{1}{F} + \frac{iB_1}{r^2} \right) \\ = -\frac{\epsilon \hat{v}}{2i} F' + \frac{r \partial_t \hat{v}}{4i} F + \frac{\kappa}{2} F' + \frac{\epsilon \kappa}{2} \left(F \psi' + \frac{iF}{r} \right), \\ \hat{\Delta}B_1 + 2 \left(F^2A_1 + \psi'F \frac{\partial A_1}{\partial r} \frac{1}{F} + \frac{iA_1}{r^2} \right) \\ = -\frac{\epsilon \hat{v}}{2i} \left(F \psi' + \frac{iF}{r} \right) - \epsilon \frac{\kappa}{2} F' + \frac{\kappa}{2} \left(F \psi' + \frac{iF}{r} \right), \end{aligned} \quad (14)$$

where $\hat{\Delta} = \partial_r^2 + r^{-1}\partial_r - r^{-2} - (\partial_r^2 F + 1/r\partial_r F)/F$ and primes denote differentiation with respect to r . Equation (14) can be formally simplified by the transformation $B_1 = \tilde{B}_1 - \epsilon r F/4$, $A_1 = \tilde{A}_1$ [26]. After simple algebra, Eqs. (14) assume the form (we omit tildes on A and B)

$$\begin{aligned} \hat{\Delta}A_1 - 2 \left(cF^2A_1 + \psi'F \frac{\partial B_1}{\partial r} \frac{1}{F} + \frac{iB_1}{r^2} \right) &= -\frac{\epsilon \bar{v}}{2i} F' + \frac{r \partial_t \hat{v}}{4i} F, \\ \hat{\Delta}B_1 + 2 \left(F^2A_1 + \psi'F \frac{\partial A_1}{\partial r} \frac{1}{F} + \frac{iA_1}{r^2} \right) &= -\frac{\epsilon \bar{v}}{2i} \left(F \psi' + \frac{iF}{r} \right), \end{aligned} \quad (15)$$

where $\bar{v} = \hat{v} - i\kappa/\epsilon$. The solvability condition for Eqs. (15) implies a unique relation between $\partial_t \hat{v}$ and \bar{v} . If the solvability condition is fulfilled, the solutions A_1 and B_1 remain finite at $r=0$ and do not grow exponentially for $r \rightarrow \infty$. Slow, powerlike growth of the solutions is permitted, since the right hand side of Eqs. (15) grows linearly with r . Thus the transformation $B_1 \rightarrow \tilde{B}_1 - \epsilon r F/4$ does not change the solvability condition. Remarkably, Eqs. (15) coincide with the equations analyzed in Ref. [6] for the case of the acceleration instability of a spiral wave in two dimensions. The only difference is that the normal velocity is modified by the curva-

ture κ . Obviously, it results in the same solvability conditions as the corresponding equations of the two-dimensional case,

$$\partial_t \hat{v} + \epsilon \chi \bar{v} = 0, \quad (16)$$

with the same ‘‘complex’’ friction coefficient χ . The equation of motion (16) can be written in the matrix form

$$\partial_t \mathbf{v} + \hat{K}[\epsilon \mathbf{v} - \kappa \mathbf{N}] = 0. \quad (17)$$

Note that, dropping the acceleration term in Eq. (17), we recover the result of Ref. [22] for $b \rightarrow \infty$, since for the ring $v_N = \partial_t R$ and $\kappa = -1/R$. Restoring the original scaling $r \rightarrow r/\sqrt{b}$, we obtain $\partial_t R = -b^2/R$. However, since in three dimensions the local velocity in general varies along the vortex line, even small acceleration may cause a severe instability of the vortex line, because the local curvature becomes very large. Moreover, deviation of the local velocity from the direction of normal will lead to a stretching and bending of the vortex line. Thus the acceleration term, which formally can be considered as a higher-order correction to the equation of the motion, may play a pivoting role in the dynamics of a vortex filament. Our subsequent analysis and numerical simulations verify this hypothesis.

B. Almost straight vortex

Let us consider an almost straight vortex parallel to the axis z . We can parametrize the position along the vortex line by the z coordinate: $[X_0(z), Y_0(z)]$. Since in this limit the arclength s is close to z , the curvature correction to the velocity $\kappa \mathbf{N}$ is simply $\kappa \mathbf{N} = (\partial_z^2 X_0, \partial_z^2 Y_0) = \partial_z^2 \mathbf{r}$, where $\mathbf{r} = (X_0, Y_0)$. Using $\partial_t \mathbf{r} = \mathbf{v}$, from Eq. (17) we then obtain

$$\partial_t \mathbf{v} + \hat{K}[\epsilon \mathbf{v} - \partial_z^2 \mathbf{r}] = \mathbf{0}, \quad (18)$$

Let us now consider perturbations of the vortex that are periodic along z . Due to the linearity of the problem, the solution can be written in the form $\mathbf{r} \sim \exp[ikz + \lambda(k)t]$, where λ is the growth rate. We immediately obtain the following relation for λ :

$$\lambda^2 + \chi(\epsilon \lambda + k^2) = 0. \quad (19)$$

Let us consider separately two cases $k \ll \epsilon$ and $k \gg \epsilon$. For $k \ll \epsilon$ from Eq. (19) we derive that $\lambda = -\epsilon \chi + O(k^2)$. For $k \gg \epsilon$ we obtain $\lambda \approx \pm \sqrt{-(K_{xx} \pm iK_{xy})}k$. There always exists a root with a large positive real part: $\lambda \sim k \gg \epsilon$. Therefore, for finite k , the growth rate $\lambda(k)$ may significantly exceed the increment of the acceleration instability in two dimensions (corresponding to $k=0$): $\lambda = -\epsilon \chi = -\epsilon(K_{xy} \pm iK_{xy})$. We can expect that, as a result of such an instability, highly curved vortex filaments will be formed. Hence the ‘‘small-curvature’’ approximation considered above can be valid only for finite time. Moreover, one may not expect this instability always to saturate in a steady-state configuration with finite curvature (although we will show this possibility to exist). In contrast, we suggest that, frequently, reconnection of various parts of the filaments, formation of vortex loops etc, will result in persistent spatiotemporal dynamics of a highly entangled vortex state. We expect a fall off of the

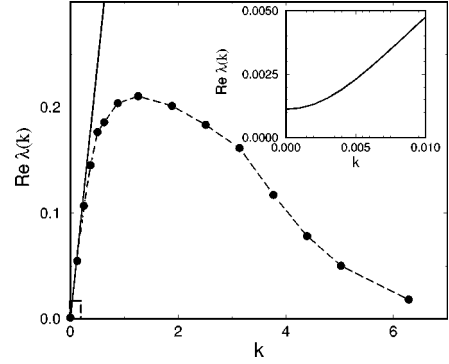


FIG. 2. The growth rate $\text{Re}\lambda(k)$ as function of k for $\epsilon = 0.02, c = 0.1$. The solid line is the theoretical result for $k \leq 1$, and the dashed line with symbols is the result of numerical solution of 3D CGLE. Inset: blowup of the small k region.

growth rate λ at large k which is not captured by the small-curvature approximation used here. This effect will be included in the treatment below.

III. NUMERICAL RESULTS

In order to verify our results numerically and to follow later development of the instability, we performed simulations of the three-dimensional CGLE. We studied a system of 50^3 – 60^3 dimensionless units of Eq. (3) with either no-flux or periodic boundary conditions. The numerical solution was implemented on a parallel 16 processors Origin 2000 computer of the High Performance Computing Center at Argonne National Laboratory. We applied an implicit Crank-Nicholson algorithm based on iteration scheme for inversion of a band matrix. The number of grid points was 100^3 – 128^3 . We performed simulations in the parameter regime away from amplitude turbulence in two dimensions [6] for various values of ϵ and c .

We numerically verified our theoretical result for the growth rate of linear perturbation for a straight vortex [Eq. (19)]. As an initial condition we selected a straight vortex line with small periodic modulation along the z axis. We have numerically measured the growth rate as a function of modulation wave number k . The results of our simulations are summarized in Fig. 2. As we see from the figure, the growth rate indeed increases initially with k , and then falls off for large k . The theoretical expression (19) shows reasonable agreement with the simulations results for small enough k . The maximum growth rate reached for intermediate values of k exceeds in this case the growth rate of the two-dimensional acceleration instability ($k=0$) by more than two orders of magnitude.

The long-time evolution of a straight vortex is shown in Fig. 3. As an initial condition we used a straight vortex perturbed by a small broadband noise. As we can see from the figure, the length of the vortex line grows. The dynamics seems to be very rapidly varying in time, and the line intersects itself many times forming numerous vortex loops. The long-time dynamics shows, however, a saturation when a highly entangled vortex state is developed and the total length of the line cannot grow further due to a repulsive interaction between closely packed line segments. The dependence of the line length on time is shown in Fig. 4. As a

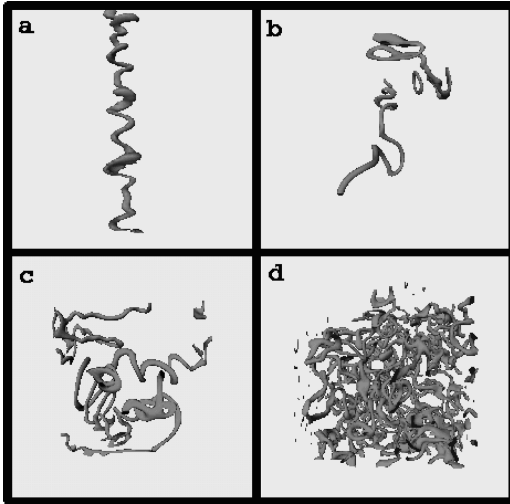


FIG. 3. Instability of a straight vortex filament. 3D isosurfaces of $|A(x, y, z)| = 0.1$ for $\epsilon = 0.02$, $c = -0.03$, are shown at four times: 50 (a), 150 (b), 250 (c), and 500 (d). A similar dynamics is also observed for a larger value of ϵ .

measure of the filament length L we used the following quantity: $L \approx S_0^{-1} \int \Theta(A_0 - |A(x, y, z)|) dx dy dz$, where Θ is the step function: $\Theta(x) = 1$ if $x > 0$ and $\Theta = 0$ otherwise. $A_0 = 0.1$ was used as a threshold value to identify the vortex. S_0 is a constant determined from the condition that for the straight line the above integral coincides with the actual length. We can identify two distinct stages of the dynamics: first, fast growth of the length; second, oscillations of the line's length around some mean value.

Strikingly, for small enough ϵ , we have observed two distinct behaviors of the total vortex length depending on the value of c . Above a critical value c_c corresponding approximately to the so-called convective instability range of the two-dimensional spiral ($c_c \rightarrow 0$ for $\epsilon \rightarrow 0$), the total length approaches some equilibrium value, and does not exhibit significant fluctuations. On the contrary, for $c < c_c$, the total length exhibits large nondecaying intermittent fluctuations around the mean value. Figure 4 demonstrates the two cases. In Fig. 5 we present snapshots illustrating the structure of the vortex field in the intermittent case corresponding to the maximum of the length [Fig. 5(a)] and the minimum [Fig. 5(b)], respectively. One sees that, in this situation, some seg-

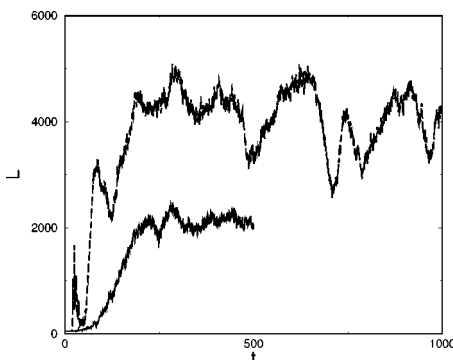


FIG. 4. The dependence of filament length L on time t . The solid line corresponds to $\epsilon = 0.02$, $c = -0.03$; the dashed line corresponds to $\epsilon = 0.02$, $c = -0.5$.

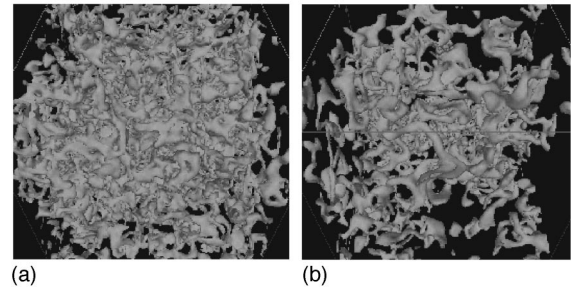


FIG. 5. Two snapshots of 3D isosurfaces of $|A|$ taken in the regime of spatiotemporal intermittency, $\epsilon = 0.02$, $c = -0.5$. (a) Left image corresponds to $t \approx 620$ for Fig. 4. (b) Right image corresponds to $t \approx 740$.

ments of vortex lines start to expand spontaneously, pushing away other vortex filaments and in such a way making substantial vortex free holes around them. Then the instability takes over and destroys these almost-straight segments of filament, bringing the system back to a highly chaotic state. This dynamics can be considered as a three-dimensional spatiotemporal vortex intermittency, which is an extension of spiral intermittency discovered in the context of the two-dimensional CGLE in Ref. [6]. For even smaller values of $c < -1$ we observed the transition to a highly chaotic state, which is an analog of “defect turbulence” in the two-dimensional CGLE. In this regime small vortex loops nucleate and annihilate spontaneously, and large vortex filaments play no role in the dynamics.

The evolution of a closed vortex loop is shown in Fig. 6. Our simulations show that the three-dimensional instability may prevent the ring from collapse, causing the stretching of the loop in the direction transversal to the the collapse motion. However, we have also found that small enough rings typically collapse, since then the instability described above does not have time to develop substantial distortions of the

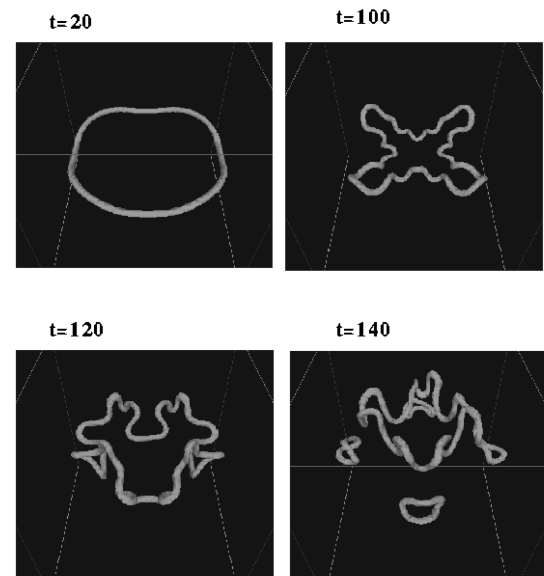


FIG. 6. Sequence of snapshots demonstrating the evolution of a vortex ring for $\epsilon = 0.2$ and $c = 0.2$.

ring. Even in this situation, the ring exhibits a few oscillations of the radius. Probably, the oscillations in the collapse rate in Fig. 2 of Ref. [22] are caused by the effect of the acceleration term in the equation of motion, which plays an important role even in the stable case.

IV. LIMITS OF THREE-DIMENSIONAL INSTABILITY

The previous analysis indicates instability of vortex lines in the limit $\epsilon \rightarrow 0$ for all c . However, it cannot describe the boundary of the instability in the c, ϵ plane since the transition to a stable regime occurs for some finite value of ϵ . In order to obtain the stability limit we performed a full linear stability analysis of a straight vortex solution, which is not limited to small k and ϵ .

The perturbative solution is of the form

$$A = [F(r) + W(r, \theta, z, t)] \exp\{i[\omega t + \theta + \psi(r)]\}. \quad (20)$$

Substituting the ansatz (20) into the CGLE, and performing the linearization with respect to W as before, then separating the real and imaginary part of W and representing the solution in the form

$$\begin{pmatrix} \text{Re}W \\ \text{Im}W \end{pmatrix} = \sum_{n=-\infty}^{\infty} \begin{pmatrix} A_n(r) \\ B_n(r) \end{pmatrix} \exp[in\theta + ikz + \lambda(k)t], \quad (21)$$

we obtain an eigenvalue problem for the eigenvalue $\lambda(k)$. Again, we restrict ourself by the analysis of most dangerous perturbation harmonics with $n=1$. The resulting equations are of the form [compare Eqs. (14) and (15)]:

$$\begin{aligned} \hat{\Delta}A_1 - k^2A_1 - 2 \left(c_1 F^2 A_1 + \psi' F \frac{\partial B_1}{\partial r} + \frac{iB_1}{r^2} \right) \\ = \frac{\lambda(k)}{1 + \epsilon^2} (\epsilon A_1 + B_1), \\ \hat{\Delta}B_1 - k^2B_1 + 2 \left(c_2 F^2 A_1 + \psi' F \frac{\partial A_1}{\partial r} + \frac{iA_1}{r^2} \right) \\ = \frac{\lambda(k)}{1 + \epsilon^2} (\epsilon B_1 - A_1), \end{aligned} \quad (22)$$

where $c_1 = (\epsilon + c)/(1 + \epsilon^2)$ and $c_2 = (1 - \epsilon c)/(1 + \epsilon^2)$. The functions A_1 and B_1 are subject to the boundary conditions: A_1 and B_1 are bounded at $r=0$, and decay exponentially for $r \rightarrow \infty$.

We solved Eqs. (22) in the range of wave numbers k numerically using a matching-shooting method with Newton iterations from NAG library, routine *d02agf*. Since Eqs. (22) are singular at $r=0$ and the solution is required on an infinite interval, we applied the following method of solution of this rather difficult eigenvalue problem. The functions A_1 and B_1 were expanded in a series for $r \rightarrow 0$, and we used the asymptotic expansion for $r \rightarrow \infty$. We replaced the boundary conditions at $r=0$ and $r \rightarrow \infty$ by new boundary conditions at sufficiently small r_0 and sufficiently large r_e . The boundary values were obtained from the corresponding asymptotic expansions, while the unknown parameters of these expansions

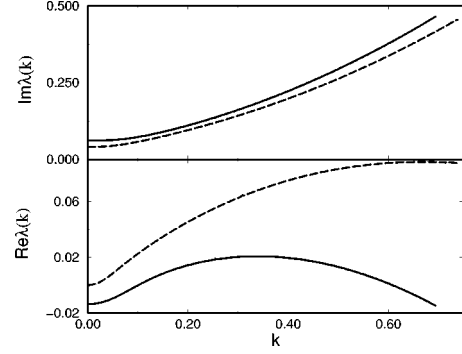


FIG. 7. $\text{Re}\lambda$ and $\text{Im}\lambda$ as functions of k for $\epsilon=0.3$ (solid line) and $\epsilon=0.14$ (dashed line) for $c=0.5$.

were included in the shooting-matching procedure. Thus the numerical matching procedure was applied on a finite interval $r_0 < r < r_e$, where r_0 was typically 10^{-2} , and r_e was gradually increased until the eigenvalue λ approaches its asymptotic value. Since the unperturbed functions F and ψ are known only numerically, we determined them in the same matching routine, solving three nonlinear equations (for F , F' , and ψ') and eight first-order linear equations (the functions A_1 and B_1 are complex). We typically used 5000 mesh points on the interval of integration.

The spectrum of $\text{Re}\lambda(k)$ for two values of ϵ is shown in Fig. 7. A typical localized core eigenmode, corresponding to this three-dimensional instability, is shown in Fig. 8. As we can see from Fig. 7, $\text{Re}\lambda(k)$ indeed falls off for large k . As expected from the previous analysis, the three-dimensional instability persists beyond the two-dimensional core instability. From Fig. 7, we see that for ϵ smaller than about 0.3 one has $\text{Re}\lambda(0) < 0$ (the core is stable in two dimensions), however there is an instability for finite k . The relation between the eigenvalue problem Eq. (22) and the acceleration instability is presented in Appendix B.

We systematically tracked the boundary for the three-dimensional instability from the condition $\max \text{Re}\lambda = 0$. The results are shown in Fig. 9. As one can see, the three-dimensional instability occurs over a much wider parameter range than the two-dimensional core instability. Moreover, the typical growth rate in three dimensions is much higher than in two dimensions.

We expect that for $c \rightarrow -\infty$ the critical line of the three-

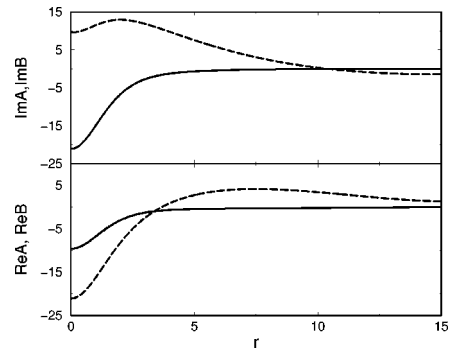


FIG. 8. $\text{Re}A_1$ and $\text{Im}A_1$ (solid lines) and $\text{Re}B_1$ and $\text{Im}B_1$ (dashed lines) as functions of r , obtained from numerical solution of Eqs. (22) for $\epsilon=0.3$, $c=0.5$, and $k=0.2$, corresponding to $\lambda = 0.0163 + i0.122$.

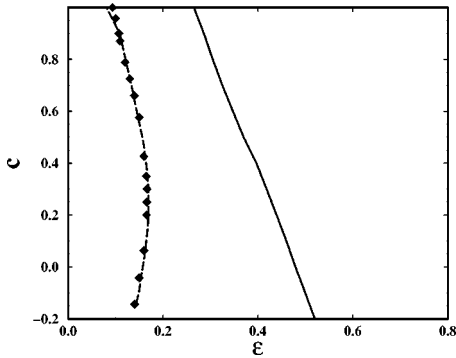


FIG. 9. Stability limits in three (solid line) and two dimensions (dashed line), obtained from linear stability analysis. Symbols represent the limit of the two-dimensional instability, obtained by direct numerical simulation of the CGLE from Ref. [6]. Vortex lines and two-dimensional spirals are stable to the right of the respective lines.

dimensional instability again approaches the $\epsilon=0$ line, similarly to the two-dimensional core instability line [6]. However, our numerical matching procedure failed to converge for this region of the parameters, since the critical mode becomes less localized for $c \rightarrow -\infty$.

V. WEAKLY NONLINEAR ANALYSIS

Our numerical simulations near the stability boundary of the three-dimensional instability have revealed a striking result: the instability saturates, leading to the formation of a stable traveling helix solution (see Fig. 10). The pitch of the helix is determined by the most unstable wavelength, and the radius of the helix vanishes when approaching the stability boundary. The existence of the stable helix solution can be considered a result of saturation of the Hopf bifurcation, which is thus of supercritical nature.

Although we have never observed saturation of the acceleration instability in two dimensions, here the situation is different, since the most unstable mode has a different spatial structure than the acceleration mode in two dimensions. The helix near the stability limit can be described in the framework of a weakly nonlinear analysis for the relevant order parameter, which characterizes the local helicity of the vortex line.

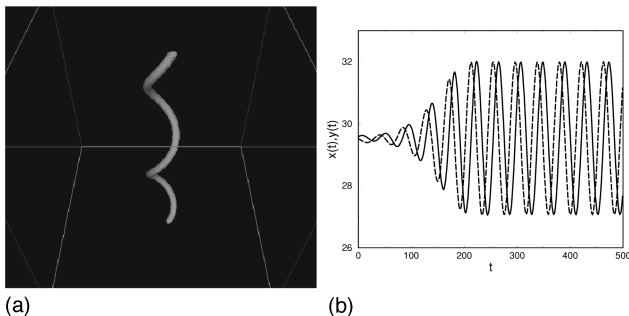


FIG. 10. (a) Stable traveling helix solution, obtained numerically for $\epsilon=0.3$ and $c=0.5$. (b) The coordinates of the vortex line $x(t)$ (solid line) and $y(t)$ (dashed line) as functions of time for some fixed z . A supercritical character of the bifurcation is apparent.

The structure of the amplitude equations can be uncovered from the following consideration. The growth rate $\lambda(k)$ is symmetric with respect to k : $\lambda(k)=\lambda(-k)$. Therefore, at the transition point two modes with k_c and $-k_c$, corresponding to counterpropagating waves of opposite helicity, simultaneously become unstable. In general, $\Omega(k)=\text{Im}\lambda(k)\neq 0$. Thus at lowest order we shall obtain two coupled one-dimensional Ginzburg-Landau equations for counterpropagating waves with the amplitudes U and V . Close to the threshold the structure of these equations becomes universal:

$$\partial_t U + v_p \partial_z U = \lambda(k_c) U + \frac{1}{2} \partial_k^2 \lambda(k_c) \partial_z^2 U - (a_1 |U|^2 + a_2 |V|^2) U,$$

$$\partial_t V - v_p \partial_z V = \lambda(k_c) V + \frac{1}{2} \partial_k^2 \lambda(k_c) \partial_z^2 V - (a_1 |V|^2 + a_2 |U|^2) V, \quad (23)$$

where $v_p = \partial_k \Omega(k_c)$, and a_1 and a_2 are complex constants. The coefficients of the linear problem can be determined from the solution of the eigenvalue problem [Eqs. (22)]. To determine the coupling coefficients $a_{1,2}$, some additional analysis is required. In principle, they can be extracted from three-dimensional simulations.

System (23) has been studied intensively in various physics contexts (see, e.g., Refs. [27–29]). It exhibits diverse types of dynamic behaviors, including traveling waves, domain walls, sinks, shocks, and spatiotemporal chaos. Thus, in our interpretation, this chaotic behavior corresponds to slow nonperiodic spatiotemporal deformations of the helicoidal structure of the vortex line.

Equations (23) are simplified drastically if one of the counterpropagating waves is suppressed, which is the case for $\text{Re} a_1 > \text{Re} a_2$. Then this system is reduced to a single one-dimensional complex Ginzburg-Landau equation, which is of the form (in a moving frame):

$$\partial_t U = \lambda(k_c) U + \frac{1}{2} \partial_k^2 \lambda(k_c) \partial_z^2 U - a_1 |U|^2 U. \quad (24)$$

We estimated the parameters of Eq. (24) from our linear analysis and simulations [see Fig. 10(b)]. We obtained $\lambda(k_c) \approx 0.02095 + i0.1431$, $\partial_k^2 \lambda(k_c)/2 = 0.311 - i0.5315$, and $a_1 = a_0^2(1 - i0.3675)$, where a_0 is a parameter which can be scaled out. For this set of parameters of the one-dimensional CGLE ($c = -0.3675$ and $b = -0.5315/0.311 \approx -1.708$), the homogeneous solution to Eq. (24) is stable, which implies the stability of a traveling helix solution. However, we can expect that for other sets of parameters of the three-dimensional CGLE, the parameters of Eq. (24) may fall into the unstable region, e.g., the range of amplitude turbulence. This would imply chaotic oscillations of the helix. We expect that these weakly nonlinear equations (23) may also serve as building blocks for the understanding of weak vortex turbulence in the CGLE in a certain region of parameters.

An interesting question in this context is the following: Could the helices form a bound state similarly to spiral waves? One could imagine a stable double-helix state, similar to the DNA molecule. We have performed a preliminary numerical investigation of the double-helix configuration. The results presented in Fig. 11 indicate that the double helix is unstable: the outer helix expands, whereas the inner helix

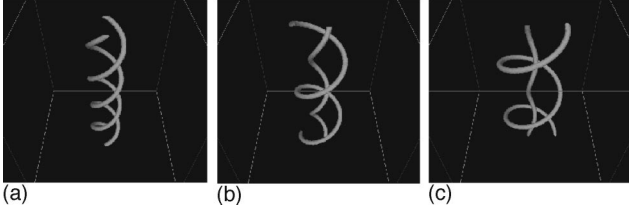


FIG. 11. Sequence of snapshots demonstrating the breakdown of a double helix for $c=0.5$ and $\epsilon=0.25$. (a) $t=60$, (b) $t=120$, and (c) $t=240$.

shrinks. However, we cannot exclude the possibility for existence of a stable double helix in some (narrow) parameter range of the CGLE.

VI. CONCLUSION

We have derived an equation of motion for the vortex line valid in the high-dispersion limit of the CGLE. Using a general linear stability analysis, we have found that in a wide range of parameters of the CGLE the vortex line is unstable with respect to spontaneous stretching and bending, resulting in the formation of persistent, dynamic entangled vortex configurations. In fact, vortex lines in three dimensions are unstable in a much wider range of parameters than two-dimensional spiral waves. This emphasizes the deficiency of previous approaches relating local filament velocity only to local curvature.

Slightly beyond the onset of the three-dimensional instability, we found stable traveling helix solutions, which bifurcate supercritically from the straight vortex. Qualitatively similar helices have recently been observed experimentally in heart tissues [30]. Note that the acceleration instability in two dimensions is subcritical [6]. Unstable helix solutions can maybe serve as building blocks for a weakly nonlinear theory of three-dimensional vortex turbulence.

Let us now discuss implication of our result for the well-known phase turbulence problem in CGLE. As was found in Ref. [31], in two dimensions phase turbulence is never a global attractor, since it is unstable with respect to invasion by defect turbulence. However, in three dimensions we may expect that at least in the region of parameters away from the stretching instability, the vortex rings collapse and the phase turbulence regains its stability. But inside the three-dimensional instability region, we may speculate that there is always a possibility for creation of a large enough vortex loop which will expand and invade the phase turbulence.

Our result could be verified in experiments with autocatalytic chemical reactions in gels in the regime of oscillatory instability. The limit of a large dispersion $b > b_c$ can probably be achieved by doping with additional chemicals, thus changing the relative mobility of reacting components.

Persistent entangled vortex configurations are known from numerical simulations of excitable reaction-diffusion systems [16,19]. Our preliminary investigation of reaction-diffusion systems shows that the underdamped core dynamics here is also responsible for long-lived vortex loops and persistent entangled vortex configuration [32]. In this case, the expansion of the vortex loops is not necessarily related to a ‘negative line tension’ of the filament, but again is the

manifestation of acceleration effects, similar to the situation in the CGLE.

Recently, the amplitude equation governing the dynamics of an elastic rod was derived [33]. The structures of solutions found in Ref. [33] are remarkably similar to those of the CGLE. It is plausible to assume that, in some distinct range of the parameters, the equations of motion of the twisted elastic rod can be reduced to the equations for the vortex line in CGLE. We also speculate that our results are relevant for inviscid hydrodynamics. In the limit of $b, c \rightarrow \infty$, Eq. (1) reduces to the defocusing nonlinear Schrödinger equation (NSE), which is a paradigm model for compressible inviscid hydrodynamics. Although the vortex lines are stable in the framework of the NSE, the corrections arising from the CGLE cause their destabilization and stretching.

ACKNOWLEDGMENTS

We are grateful to A. Newell, D. Levermore, C. Doering, R. Goldstein, L. Pismen, and W. Zimmermann for illuminating discussions. The hospitality of the Max Planck Institute for the Physics of Complex System at Dresden, where part of the work was performed, is greatly appreciated. Most of the computations were performed at the HPCC of ANL. This work was supported by the U.S. Department of Energy under Contract Nos. W-31-109-ENG-38 (I.A.) and ERW-E420 (A.B.). The work of I.A. was also supported by the NSF, Office of STC under Contract No. DMR91-20000.

APPENDIX A: LIMIT OF NONLINEAR SCHRÖDINGER EQUATION

1. Adjoint mode

In order to derive the friction coefficient χ in Eq. (16), we have to fulfill the solvability condition. In Sec. II, this was done numerically. The solvability condition means the orthogonality of the right-hand side of Eq. (15) to the adjoint mode of Eq. (15). The adjoint equations are of the forms

$$\begin{aligned} \hat{\Delta} A_1^\dagger - 2 \left(c F^2 A_1^\dagger + \frac{1}{rF} \frac{\partial}{\partial r} (r \psi' F B_1^\dagger) - \frac{i B_1^\dagger}{r^2} \right) + 2 F^2 B_1^\dagger &= 0 \\ \hat{\Delta} B_1^\dagger + 2 \left(\frac{1}{rF} \frac{\partial}{\partial r} (r \psi' F A_1^\dagger) - \frac{i A_1^\dagger}{r^2} \right) &= 0. \end{aligned} \quad (\text{A1})$$

The solvability condition of Eqs. (15) can be expressed in terms of functions A_1^\dagger and B_1^\dagger :

$$\partial_t \hat{v} I_1 - 2 \epsilon \bar{v} I_2 = 0, \quad (\text{A2})$$

where

$$\begin{aligned} I_1 &= \int_0^\infty r^2 dr F A_1^\dagger \\ I_2 &= \int_0^\infty r dr [F' A_1^\dagger + (F \psi' + i F/r) B_1^\dagger]. \end{aligned} \quad (\text{A3})$$

From Eq. (A2), we readily obtain the friction coefficient [compare with Eq. (8)]

$$\chi = -2I_2/I_1. \quad (\text{A4})$$

For arbitrary c the localized adjoint modes A_1^\dagger and B_1^\dagger can be determined only numerically [6]. However, for $c \rightarrow \infty$, i.e., in the limit of the perturbed NSE, the adjoint mode, and χ , can be calculated fully analytically. For $c \rightarrow \infty$ the selected wave number k_0 vanishes (see, e.g., Ref. [25]), the solution approaches the vortex solution of NSE, and Eq. (A1) becomes self-adjoint. We introduce a small parameter $\mu = 1/c \ll 1$ and assume $\mu \gg \epsilon$. Equations (A1) read

$$\begin{aligned} \hat{\Delta}A_1^\dagger - 2 \left(\frac{F^2}{\mu} A_1^\dagger + \frac{1}{rF} \frac{\partial}{\partial r} (r\psi' F B_1^\dagger) - \frac{iB_1^\dagger}{r^2} \right) + 2F^2 B_1^\dagger &= 0, \\ \hat{\Delta}B_1^\dagger + 2 \left(\frac{1}{rF} \frac{\partial}{\partial r} (r\psi' F A_1^\dagger) - \frac{iA_1^\dagger}{r^2} \right) &= 0. \end{aligned} \quad (\text{A5})$$

For $\mu = 0$, Eqs. (A5) are self-adjoint, and the localized adjoint eigenmode coincides with the complex-conjugated translation mode

$$\begin{pmatrix} A_1^\dagger \\ B_1^\dagger \end{pmatrix} = \begin{pmatrix} F' \\ -iF/r \end{pmatrix}. \quad (\text{A6})$$

In order to evaluate Eqs. (A4) we take into account that for any $\mu \neq 0$ the functions A_1^\dagger and B_1^\dagger decay exponentially for $r \rightarrow \infty$. Therefore, Eq. (A6) can be considered an approximation valid within a finite interval $0 < r < R_0$, where the cutoff $R_0 \gg 1$ will be determined from the matching condition with the outer asymptotics of the solution. For $r \rightarrow \infty$ we can simplify Eqs. (A5) using that $F^2 \rightarrow 1 - \mu/r^2 + \dots$, $\psi' \rightarrow k_0$ and $k_0 \ll 1$:

$$\begin{aligned} \hat{\Delta}A_1^\dagger - 2 \left(\frac{1}{\mu} A_1^\dagger + \frac{1}{r} \frac{\partial}{\partial r} (r\psi' B_1^\dagger) - \frac{iB_1^\dagger}{r^2} \right) + 2B_1^\dagger &= 0 \\ \hat{\Delta}B_1^\dagger + 2 \left(\frac{1}{r} \frac{\partial}{\partial r} (r\psi' A_1^\dagger) - \frac{iA_1^\dagger}{r^2} \right) &= 0. \end{aligned} \quad (\text{A7})$$

From the first Eq. (A7) we can explicitly express A_1^\dagger in terms of B_1^\dagger , because $r \rightarrow \infty$ for all terms in the first Eq. (A7) except A_1^\dagger/μ and B_1^\dagger . In the first relevant order we obtain

$$A_1^\dagger = \mu B_1^\dagger \quad (\text{A8})$$

Substituting now Eq. (A8) into the second equation (A7), and dropping higher-order terms, one has

$$\partial_r^2 B_1^\dagger + \frac{1}{r} \partial_r B_1^\dagger - \frac{1}{r^2} B_1^\dagger + \frac{2\mu}{r} \frac{\partial}{\partial r} (r\psi' B_1^\dagger) = 0. \quad (\text{A9})$$

Equation (A9) is reduced to Bessel's equation by the substitution $B_1^\dagger = S \exp(-\mu\psi)$, leading to

$$\partial_r^2 S + \frac{1}{r} \partial_r S - \left(\mu^2 k_0^2 + \frac{1}{r^2} \right) S = 0. \quad (\text{A10})$$

It has the localized solution $S = K_1(\mu k_0 r)$. Thus the outer solution is of the form:

$$\begin{pmatrix} A_1^\dagger \\ B_1^\dagger \end{pmatrix} = C \begin{pmatrix} \mu \\ 1 \end{pmatrix} \exp(-\psi) K_1(\mu k_0 r), \quad (\text{A11})$$

where C is a constant determined from the matching with the inner solution Eq. (A6). For $r \rightarrow \infty$ the functions decay exponentially: $A_1^\dagger, B_1^\dagger \sim \exp[-2\mu|k_0|r]/r^{1/2}$, since $\psi \rightarrow k_0 r$. The solutions (A6) and (A11) match in the intermediate region $r \gg 1$ and $\mu k_0 r \ll 1$. Expanding $K_1(\mu k_0 r)$ for small arguments, we find $C = -i\mu k_0$.

2. Friction coefficient

To calculate the integrals (A3) we introduce the cutoff $R_0 = 1/(\mu k_0) \gg 1$ and split the interval of integration into two parts: $0 < r < R_0$ and $R_0 < r < \infty$. In the first interval we use the inner representation of the eigenfunctions [Eq. (A6)], and in the second one the outer representation [Eq. (A11)]. For the inner interval we obtain

$$\begin{aligned} I_1^i &= \int_0^{R_0} r^2 dr F F' = b_0 + \mu \ln R_0 \\ I_2^i &= \int_0^{R_0} r dr [(F')^2 + (F/r)^2] = b_1 + \ln R_0, \end{aligned} \quad (\text{A12})$$

where b_0 and b_1 are some constants. From the outer integration for I_2 , we have [using $\psi' \rightarrow k, F \rightarrow 1$ for $r \rightarrow \infty$, see Eq. (A3)]

$$I_2^o \approx \int_{R_0}^{\infty} r (k_0 + i/r) dr B_1^\dagger \approx -0.884 - \ln(R_0 \mu k_0) - i0.666/\mu. \quad (\text{A13})$$

In order to evaluate the integral I_1^o , we need the next order of the function A_1^\dagger to compensate for the logarithmic divergence of the inner integral. From Eq. (A5) we obtain $A_1^\dagger = \mu(B_1^\dagger + iB_1^\dagger/r^2)$. Thus we have

$$\begin{aligned} I_1^o &= \int_{R_0}^{\infty} r^2 dr \left[-i\mu k_0 \left(1 + \frac{i}{r^2} \right) \right] \mu K_1(\mu k_0 r) \exp(\mu k_0 r) \\ &\approx -0.884\mu - \mu \ln(R_0 \mu k_0) - \frac{0.4i}{\mu k_0^2}. \end{aligned} \quad (\text{A14})$$

Combining now the outer and inner expansions, we see that R_0 drops out. The friction coefficient is of the form:

$$\chi = -2 \frac{-\ln(\mu k_0) + c_1 - i0.666/\mu}{-\mu \ln(\mu k_0) + c_0 - i0.4/(\mu k_0^2)}, \quad (\text{A15})$$

where $c_1 = b_1 - 0.884$ and $c_0 = b_0 - 0.884\mu$. Now, using Hagan's expression for the selected wave number [25] in our scaling of the CGLE parameters, one finds $k_0 \approx 2\mu^{-3/2} \exp[-\pi/(2\mu) - \gamma - 0.098]$. We finally obtain

$$\chi \approx -\frac{13.3}{\mu^3} \exp\left(-\frac{\pi}{\mu} - 2\gamma - 0.196\right) \left(1 + \frac{i\pi}{0.8}\right)$$

$$\approx -\frac{3.45}{\mu^3} \exp\left(-\frac{\pi}{\mu}\right) (1 + 3.92i). \quad (\text{A16})$$

The real part of the friction coefficient is always negative, which implies the instability of the spiral core in two dimensions and a stretching instability in three dimensions.

APPENDIX B: RELATION BETWEEN ACCELERATION INSTABILITY AND STABILITY PROBLEMS

The result of Sec. II for weakly curved vortex filaments can be formally derived from the linear stability problem [Eq. (22)] through systematic expansion in ϵ up to second order. The eigenvalue problem for $\epsilon \ll \mu$ is of the form

$$\hat{\Delta}A_1 - 2\left(\frac{1}{\mu}F^2A_1 + \psi'F\frac{\partial}{\partial r}\frac{B_1}{F} + \frac{iB_1}{r^2}\right) = (\lambda\epsilon + k^2)A_1 + \lambda B_1, \quad (\text{B1})$$

$$\hat{\Delta}B_1 + 2\left(F^2A_1 + \psi'F\frac{\partial}{\partial r}\frac{A_1}{F} + \frac{iA_1}{r^2}\right) = (\lambda\epsilon + k^2)B_1 - \lambda A_1$$

Now we expand Eq. (B1) in ϵ . The solution is represented in the form

$$\begin{pmatrix} A_1 \\ B_1 \end{pmatrix} = \begin{pmatrix} A^{(0)} \\ B^{(0)} \end{pmatrix} + \epsilon \begin{pmatrix} A^{(1)} \\ B^{(1)} \end{pmatrix} + \dots, \quad (\text{B2})$$

$$\lambda = \epsilon\lambda^{(1)} + \epsilon^2\lambda^{(2)} + \dots$$

We consider $k \sim O(\epsilon)$, and denote $\bar{k} = k/\epsilon$.

At zeroth order in ϵ we simply obtain $\hat{L}(A^{(0)}, B^{(0)}) = 0$, where \hat{L} is the right hand side of Eqs. (B1). Clearly the solution is the translation mode

$$\begin{pmatrix} A^{(0)} \\ B^{(0)} \end{pmatrix} = \begin{pmatrix} F' \\ F\psi' + \frac{iF}{r} \end{pmatrix}. \quad (\text{B3})$$

At first order in ϵ , we obtain

$$\hat{L}\begin{pmatrix} A^{(1)} \\ B^{(1)} \end{pmatrix} = \lambda^{(1)} \begin{pmatrix} F\psi' + \frac{iF}{r} \\ -F' \end{pmatrix}. \quad (\text{B4})$$

The equations have an exact solution corresponding to the ‘‘family mode,’’ which exists for $\epsilon = 0$:

$$\begin{pmatrix} A^{(1)} \\ B^{(1)} \end{pmatrix} = -\frac{\lambda^{(1)}}{2} \begin{pmatrix} 0 \\ rF' \end{pmatrix}. \quad (\text{B5})$$

At second order in ϵ , we obtain equations

$$\hat{L}\begin{pmatrix} A^{(2)} \\ B^{(2)} \end{pmatrix} = \begin{pmatrix} (\lambda^{(1)} + \bar{k}^2)F' - \frac{(\lambda^{(1)})^2}{2}rF \\ (\lambda^{(1)} + \bar{k}^2)\left(F\psi' + \frac{iF}{r}\right) \end{pmatrix} + \lambda^{(2)} \begin{pmatrix} B^{(0)} \\ -A^{(0)} \end{pmatrix}. \quad (\text{B6})$$

These equations have a bounded solution if the solvability condition is satisfied. It is easy to see that Eqs. (B6) are identical to Eqs. (15) if we take into account $\hat{v} \sim \lambda, \partial_r \hat{v} = \lambda \hat{v}$ and $\kappa = k^2$. The solvability condition implies that $(\lambda^{(1)})^2 + \chi(\lambda^{(1)} + k^2) = 0$. The last term in Eqs. (B6) can be omitted, since it generates a nonsingular solution [family mode, compare Eq. (B5)]. Thus we reproduce the result for a weakly curved vortex [Eq. (19)].

-
- [1] A. C. Newell, *Envelope Equations* (American Mathematical Society, Providence, RI, 1974).
- [2] Y. Kuramoto, *Chemical Oscillations, Waves and Turbulence* (Springer-Verlag, Berlin, 1983).
- [3] M. Cross and P. C. Hohenberg, *Rev. Mod. Phys.* **65**, 851 (1993).
- [4] I. Aranson, L. Aranson, L. Kramer, and A. Weber, *Phys. Rev. A* **46**, R2992 (1992).
- [5] I. Aranson, L. Kramer, and A. Weber, *Phys. Rev. E* **47**, 3231 (1993); **48**, R9 (1993).
- [6] I. Aranson, L. Kramer, and A. Weber, *Phys. Rev. Lett.* **72**, 2316 (1994).
- [7] G. Huber, P. Alstr m, and T. Bohr, *Phys. Rev. Lett.* **69**, 2380 (1992); H. Chat  and P. Manneville, *Physica A* **224**, 348 (1996).
- [8] F. T. Arrecchi *et al.*, *Phys. Rev. Lett.* **67**, 3749 (1991).
- [9] Q. Ouyang and J.-M. Flesselles, *Nature (London)* **379**, 6561 (1996).
- [10] M. Ruiz-Villareal, M. Gomez-Gesteira, and V. Perez-Villar, *Phys. Rev. Lett.* **78**, 779 (1997).
- [11] I. Aranson, H. Levine, and L. Tsimring, *Phys. Rev. Lett.* **72**, 2561 (1994).
- [12] K. J. Lee, E. C. Cox, and R. E. Goldstein, *Phys. Rev. Lett.* **76**, 1174 (1996).
- [13] F. Siegert and C. J. Weijer, *Proc. Natl. Acad. Sci. USA* **89**, 6433 (1992).
- [14] R. A. Gray and J. Jalife, *Int. J. Bifurcation Chaos Appl. Sci. Eng.* **6**, 415 (1996).
- [15] M. Wilson, S. Mironov, S. Mulvey, and A. Pertsov, *Nature (London)* **386**, 477 (1997).
- [16] A. T. Winfree, *Physica D* **84**, 126 (1995).
- [17] A. T. Winfree *et al.*, *Chaos* **6**, 617 (1996).
- [18] V. N. Biktashev, A. V. Holden, and H. Zhang, *Philos. Trans. R. Soc. London, Ser. A* **347**, 611 (1994).
- [19] F. Fenton and A. Karma (unpublished).
- [20] J. P. Keener, *Physica D* **31**, 269 (1988).
- [21] T. Frisch and S. Rica, *Physica D* **61**, 155 (1992).
- [22] M. Gabbay, E. Ott, and P. Guzdar, *Phys. Rev. Lett.* **78**, 2012 (1997).
- [23] I. S. Aranson and A. R. Bishop, *Phys. Rev. Lett.* **79**, 4174 (1997).
- [24] J. Lega, J. V. Moloney, and A. C. Newell, *Phys. Rev. Lett.* **73**, 2978 (1994).

- [25] P. Hagan, SIAM (Soc. Ind. Appl. Math.) J. Appl. Math. **42**, 762 (1982).
- [26] The hint for this substitution can be obtained from the expansion of solution $A_0 \exp[i\delta k_x x] = A_0 + i\delta k_x x A_0$, found in Ref. [22], where A_0 is unperturbed spiral solution.
- [27] I. Aranson and L. Tsimring, Phys. Rev. Lett. **75**, 3273 (1995).
- [28] R. Alvarez, M. van Hecke, and W. van Saarloos, Phys. Rev. E **56**, R1306 (1997).
- [29] H. Riecke and L. Kramer (unpublished).
- [30] S. Mironov, M. Vinson, S. Mulvey, and A. Pertsov, J. Phys. Chem. **100**, 1975 (1996).
- [31] P. Manneville and H. Chatê, Physica D **96**, 30 (1995).
- [32] I. Aranson and I. Mitkov (unpublished).
- [33] A. Goriely and M. Tabor, Phys. Rev. Lett. **77**, 3537 (1997); Physica D **105**, 20 (1997).